Carbon 139 (2018) 896–905

Contents lists available at ScienceDirect

Carbon

journal homepage: www.elsevier.com/locate/carbon

Ultrathin HfO_2-modified carbon nanotube films as efficient polysulfide barriers for Li-S batteries

Weibang Kong [a, c], Datao Wang [a], Lingjia Yan [a], Yufeng Luo [a], Kaili Jiang [a, b], Qunqing Li [a, b], Li Zhang [c], Shigang Lu [c], Shoushan Fan [a], Ju Li [d], Jiaping Wang [a, b, d, *]

[a] Department of Physics and Tsinghua-Foxconn Nanotechnology Research Center, Tsinghua University, Beijing 100084, China
[b] Collaborative Innovation Center of Quantum Matter, Beijing 100084, China
[c] China Automotive Battery Research Institute, Beijing 100088, China
[d] Department of Nuclear Science and Engineering and Department of Materials Science and Engineering, Massachusetts Institute of Technology, Cambridge, MA 02139, USA

ARTICLE INFO

Article history:
Received 23 April 2018
Received in revised form
18 July 2018
Accepted 28 July 2018
Available online 30 July 2018

Keywords:
Hafnium oxide
Carbon nanotube
Interlayer
Polysulfide
Li–S battery

ABSTRACT

Ultrathin and cross-stacked carbon nanotube (CNT) films modified with hafnium oxide (HfO_2) by atomic layer deposition are employed as efficient polysulfide barriers for high performance Li-S batteries. A HfO_2/CNT interlayer has an ultrathin, flexible structure with a thickness of 1.5 μm and an areal density of 0.087 mg cm^{-2}, along with excellent wettability to electrolyte. The highly conductive CNT network and the catalytic surface adsorption of polysulfide species by HfO_2 significantly suppress the polysulfides shuttling phenomenon. With high sulfur loadings of up to 75 wt%, electrodes incorporating a HfO_2/CNT interlayer show noticeable improvements in various electrochemical properties, including long-term cycling stability (721 mA h g^{-1} after 500 cycles at 1 C), high rate performance (800 mA h g^{-1} at 5 C), favorable anti-self-discharge capabilities, and suppression of Li anode corrosion. These results suggest a new and efficient polysulfide trapping material and a viable configuration for high-performance Li-S batteries.

1. Introduction

The rapid development of portable electronic devices and electric vehicles has led to demands for further research on energy storage systems with high energy densities and long service lives. Conventional lithium ion batteries have approached their ceiling performance due to the limited theoretical capacity of the electrode materials in these devices [1,2]. Lithium sulfur (Li-S) batteries are considered as one of the most promising types of next-generation devices, due to the high theoretical specific capacity (1672 mA h g^{-1}) and gravimetric energy density (2600 W h kg^{-1}) of sulfur. In addition, the natural abundance, low cost, and minimal toxicity of sulfur make Li-S batteries even more attractive [3,4]. However, the commercial development of Li-S batteries is hampered by several problems, including rapid capacity degradation and low sulfur utilization. The key issues are related to the insulating nature of sulfur and its various discharge products, the large volume expansion upon discharge (80%) of the electrodes, and the dissolution of intermediate long-chain polysulfides (Li_2S_n, $4 \leq n \leq 8$) generated during the charge/discharge processes. The dissolved polysulfides shuttle between the electrodes, leading to a series of side-reactions and poor cycling/rate performance (known as the shuttle effect), which remains a major challenge associated with Li-S batteries [5,6].

To address these problems, various approaches have been proposed to develop novel Li-S cell configurations in recent years. The main strategy has been to design effective composite cathodes to constrain sulfur or polysulfides within a porous nanostructure. Various carbon materials, such as micro/mesoporous carbons [7–9], hollow carbon nanospheres [10,11], carbon nanotubes (CNTs) [12–14], and graphene nanosheets [15–17], have been explored as components of novel composite electrodes. These porous carbon materials with high electrical conductivity not only reduce the diffusion of polysulfides but also promote the mechanical and electrochemical integrity of the electrodes. Among these materials, super-aligned CNTs (SACNTs) stand out as a

* Corresponding author. Department of Physics and Tsinghua-Foxconn Nanotechnology Research Center, Tsinghua University, Beijing 100084, China.
E-mail address: jpwang@tsinghua.edu.cn (J. Wang).

https://doi.org/10.1016/j.carbon.2018.07.063
0008-6223/

potential sulfur-host material due to their unique structure and excellent physical properties [14,18–20]. As a result of the strong van der Waals force between the tubes, SACNTs can be drawn into ultrathin films, and thus are pivotal in the development of high-performance, flexible energy-storage devices [21–24]. When used in Li-S batteries, an interwoven SACNT network can provide mechanical support to accommodate the volume expansion of sulfur as well as continuous conductive pathways that enhance the adsorption and conversion of polysulfides.

Another notable strategy is to construct an effective polysulfide-blocking interlayer next to the separator in the battery. The ideal interlayer should have selective permeability, allowing Li ions to transport bidirectionally while restricting polysulfide diffusion [25]. Various interlayers have been proposed, including polymer membranes [26,27], porous carbons [28,29], CNTs [30,31], graphene oxides [19,32], and metal oxides/sulfides [33–35]. Among these, metal oxides/sulfides have recently received significant attention, as the nanostructured polar sites in these materials are able to strongly adsorb polysulfide intermediates [36–41]. As an example, Nazar and co-workers reported that nanostructured MnO_2 reacted with polysulfides to form surface-bound intermediates, thus reducing the shuttle effect [38]. Tang and co-workers fabricated a MoS_2/Celgard composite separator to prevent polysulfide migration to the anode, and the resulting data suggested a Mo-S_n^{2-} interaction during cycling [35]. Similar phenomena have been reported based on work with other metal oxides/sulfides, including TiO_2 [33], Al_2O_3 [34], ZrO_2 [39], CoS_2 [40] and FeS_2 [41]. Although these materials exhibit effective chemical adsorption of polysulfides, the intrinsically low conductivities of the oxides/sulfides adversely affect the electrochemical kinetics of the electrodes, especially at high sulfur loadings. Therefore, further research must focus on two issues: (1) developing more effective polysulfide trapping host materials with controlled morphologies to increase the interfacial interaction between the components, and (2) increasing conductivity of the Li-S system and catalytic conversion of polysulfides for enhanced electrochemical performance.

In this study, we developed ultrathin HfO_2-modified cross-stacked CNT interlayers for use in Li-S batteries using the atomic layer deposition (ALD) technique (Fig. 1a). Previous studies have demonstrated that HfO_2 enhances the interfacial redox reaction during electrochemical processes [42,43]. As an example, Yesibolati and co-workers confirmed that a HfO_2 layer interacted with a SnO_2 anode to improve its electrochemical performance [43]. Despite this, HfO_2 represents a novel metal oxide that has rarely been used in Li-S batteries, and the work presented herein shows that a HfO_2 nano-coating on a CNT network exhibits significant polysulfide trapping capability. By employing the ALD technique to allow precise thickness control, a high quality HfO_2 layer was obtained that demonstrated a uniform morphology together with negligible weight. Moreover, the highly conductive CNT films not only provided homogeneous templates with large surface areas for HfO_2 deposition but also efficiently accelerated charge transfer, thus promoting surface adsorption and conversion between polysulfides and HfO_2. The HfO_2/CNT interlayer had an ultrathin film structure with a low areal density of 0.087 mg cm^{-2} and showed excellent wettability to electrolyte. In addition, no current collector or polymeric binder was required in the cathode structure, and a sulfur content as high as 75 wt% was possible. As a result of the highly conductive CNT network and the polysulfide trapping ability originating from the HfO_2 modification, the HfO_2/CNT interlayer produces a remarkable improvement in the electrochemical performance of sulfur electrodes.

2. Experimental section

2.1. Synthesis of the HfO_2/CNT interlayer

SACNT arrays with diameters of 10–20 nm and heights of 300 μm were synthesized on silicon wafers by chemical vapor deposition, using Fe as the catalyst and acetylene as the precursor [21,22]. A continuous CNT sheet was drawn from the SACNT arrays via an end-to-end joining process. The fabrication of the HfO_2/CNT interlayer is illustrated in Fig. 1c. In the first step, five CNT sheet layers were cross-stacked on a 10 cm × 10 cm metal frame. These layers were subsequently exposed to an O_2 plasma to create defects on the CNT surfaces, using a reaction ion etching (RIE) system (Anelva, Japan) with a pressure of 10 Pa, a power of 20 W, and an O_2 flow rate of 40 sccm. The etching time was fixed at 10 s. Following this, the plasma-treated CNT film was coated with a thin HfO_2 layer using an ALD system (TFS200, Beneq, Finland). Hafnium tetrachloride ($HfCl_4$) gas and water vapor (H_2O) were used as the hafnium and oxygen precursors and were sequentially supplied to the deposition chamber to grow HfO_2 in a layer-by-layer manner at 200 °C, employing 14, 21, or 35 cycles. One cycle consisted of exposure to $HfCl_4$ for 0.5 s, pumping for 2 s, exposure to H_2O for 0.25 s, and pumping for 1 s. The flow rate of the carrier gas was maintained at 200 sccm throughout and the HfO_2 deposition rate was 0.1–0.2 nm per cycle. Finally, four sets of such films were stacked on a pristine separator (Polypropylene, Celgard 2400) to obtain a 20 layer HfO_2/CNT film. The average areal density of the HfO_2/CNT interlayer was only 0.087 mg cm^{-2}.

2.2. Fabrication of the S-CNT composite electrodes

SACNTs were oxidized in a mixed HNO_3/H_2SO_4 solution (3:1 weight ratio) at 80 °C for 4 h to obtain oxidized CNTs (oCNTs). Sulfur powder (Beijing Dk Nano Technology Co., Ltd) and oCNTs were dispersed in ethanol by intensive ultrasonication (1000 W) for 30 min. A binder-free and flexible S-CNT film with a uniform dispersion of sulfur nanoparticles on the oCNTs was obtained by vacuum infiltration and drying at 50 °C. The S-CNT film was subsequently sealed in a steel container and heat-treated at 155 °C for 8 h. Sulfur loadings in the composite electrodes varied between 65 and 75 wt%, corresponding to areal sulfur densities of 1.80–2.22 mg cm^{-2}. Owing to the incorporation of the highly conductive interwoven CNT network, the S-CNT composite electrodes were highly flexible and it was not necessary to include a binder or current collector (Fig. S1).

2.3. Characterization

Thermogravimetric analysis (TGA, Pyris 1, PerkinElmer, USA) of the S-CNT composite electrodes was conducted at a heating rate of 10 °C min^{-1} in air from 25 to 500 °C. The morphologies and structures of the HfO_2/CNT interlayers and S-CNT composite electrodes were investigated using scanning electron microscopy (SEM, Sirion 200, FEI) and transmission electron microscopy (TEM, Tecnai G2F20, FEI). Coin-type (CR 2016) half-cells with S-CNT composite as the working electrode and pure Li foil as the reference electrode were assembled in a glove box (M. Braun Inert Gas Systems Co., Ltd., Germany) filled with argon. The HfO_2/CNT interlayer-coated polypropylene film (Celgard 2400) was used as a separator, with the HfO_2/CNT interlayer adjacent to the S-CNT composite cathode. 1 M lithium bis(trifluoromethanesulfonyl)imide (LiTFSI) solution and 0.2 M $LiNO_3$ in a mixture of 1–3 dioxolane (DOL) and 1,2-dimethoxyethane (DME) (volume ratio 1:1) were used as the

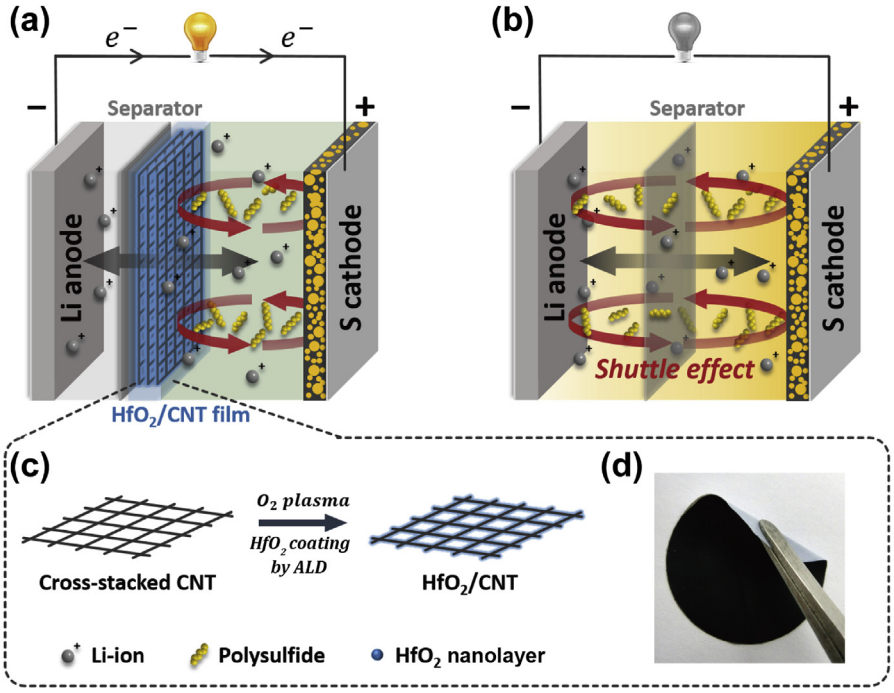

Fig. 1. Schematics of Li-S cells with (a) a HfO_2/CNT interlayer and (b) a pristine separator. (c) Schematic of the process for fabricating a HfO_2/CNT interlayer. (d) Photograph of a separator coated with a HfO_2/CNT interlayer. (A colour version of this figure can be viewed online.)

electrolyte. The ratio of electrolyte and sulfur used in the cell was 25 μL mg^{-1}. Cycling tests were performed with a Land battery test system (Wuhan Land Electronic Co., China) over the voltage window of 1.8–2.6 V at various charge/discharge rates. X-ray photoelectron spectroscopy (XPS) analysis of the HfO_2/CNT interlayer was performed using a PHI Quantera SXM instrument (ULVAC-PHI, Japan) after washing it with DOL/DME. All spectra were fitted with Gaussian–Lorentzian functions and a Shirley-type background. The binding energy values were all calibrated using the C 1s peak at 284.8 eV.

3. Results and discussion

Fig. 1a presents a schematic diagram of a Li-S cell with the HfO_2/CNT interlayer. In this design, the polysulfides generated during the charge/discharge processes can be trapped by the HfO_2/CNT interlayer to suppress the shuttle effect, while Li ions can transfer through the separator/interlayer to guarantee a stable redox reaction. On the contrary, a conventional Li-S cell with a pristine separator exhibits severe loss of active materials due to polysulfide diffusion (Fig. 1b). As noted, the cross-stacked CNT film was treated with O_2 plasma using the RIE method, such that homogeneous oxygen defects were introduced on the CNT surfaces. The aim was to provide adsorption sites for the precursors during the HfO_2 deposition process and thus ensure a uniform HfO_2 coating on the CNTs. Fig. 1d shows a photograph of a separator coated with the HfO_2/CNT interlayer. Due to the excellent mechanical properties of the interwoven CNT film, the HfO_2/CNT interlayer demonstrated high flexibility.

The O_2-based RIE treatment of the CNT film was vital for obtaining homogenous HfO_2/CNT composites. TEM images of the original CNTs (Fig. S2a) demonstrate a smooth, clean surface morphology with limited amorphous carbon deposition on the tube surfaces. In contrast, the outer layers of the RIE-treated CNTs were etched by the O_2 plasma, and oxygen groups were evenly introduced onto the surfaces (Fig. S2b). Energy dispersive X-ray (EDX) results showed that the oxygen concentration in the RIE-treated CNTs was 2.64 wt% (Fig. S2b inset). The deposition of HfO_2 via ALD required the effective adsorption of the precursors on the CNT surfaces. Fig. S3a presents a TEM image of the original CNTs following 14 ALD cycles. The HfO_2 evidently nucleated at the active sites at which amorphous carbon structures were located, and isolated HfO_2 nanoparticles can be seen along the tubes. The clean surface of the original CNTs could adsorb very little of the $HfCl_4$ precursors, and thus hindered the uniform growth of the HfO_2 layer. In contrast, when the RIE-treated CNTs underwent the same ALD procedure, a smooth, uniform HfO_2 layer resulted, with a thickness of less than 2 nm (Fig. S3b). These results suggest that the RIE treatment was critical to the homogenous deposition of HfO_2. Therefore, the CNT films used in this work were all pre-treated using RIE prior to the ALD procedure in order to obtain a uniform HfO_2 coating.

The SEM image in Fig. 2a shows the top surface of the HfO_2/CNT interlayer. Because of the ordered and cross-stacked CNT network, the interlayer had a smooth micro-porous structure. The cross-sectional SEM image in Fig. 2b demonstrates that the thickness of the HfO_2/CNT interlayer made using 21 ALD cycles was 1.5 μm. The areal density of the ultrathin interlayer was only 0.087 mg cm^{-2}. Fig. 2c presents a TEM image of the HfO_2/CNT composite and demonstrates that a thin HfO_2 layer with a thickness of approximately 3 nm was uniformly coated on the CNT surfaces. The corresponding EDX analysis demonstrated that C, O, and Hf were homogeneously distributed over the composite, further confirming a uniform HfO_2 layer. The well-dispersed conductive CNT network and the ultrathin HfO_2 layer increased the contact area between the polysulfides and the HfO_2/CNT interlayer and promoted surface adsorptive reactions between the polysulfides and the HfO_2/CNT interlayer. The wettability of separator affects the inner resistance of the cell, and the wetting speed is affected by the surface energy and porosity. Due to the high surface tension and polarization of water, wettability tests are generally performed by measuring the contact angle of the deionized water droplet on substrates [44–46].

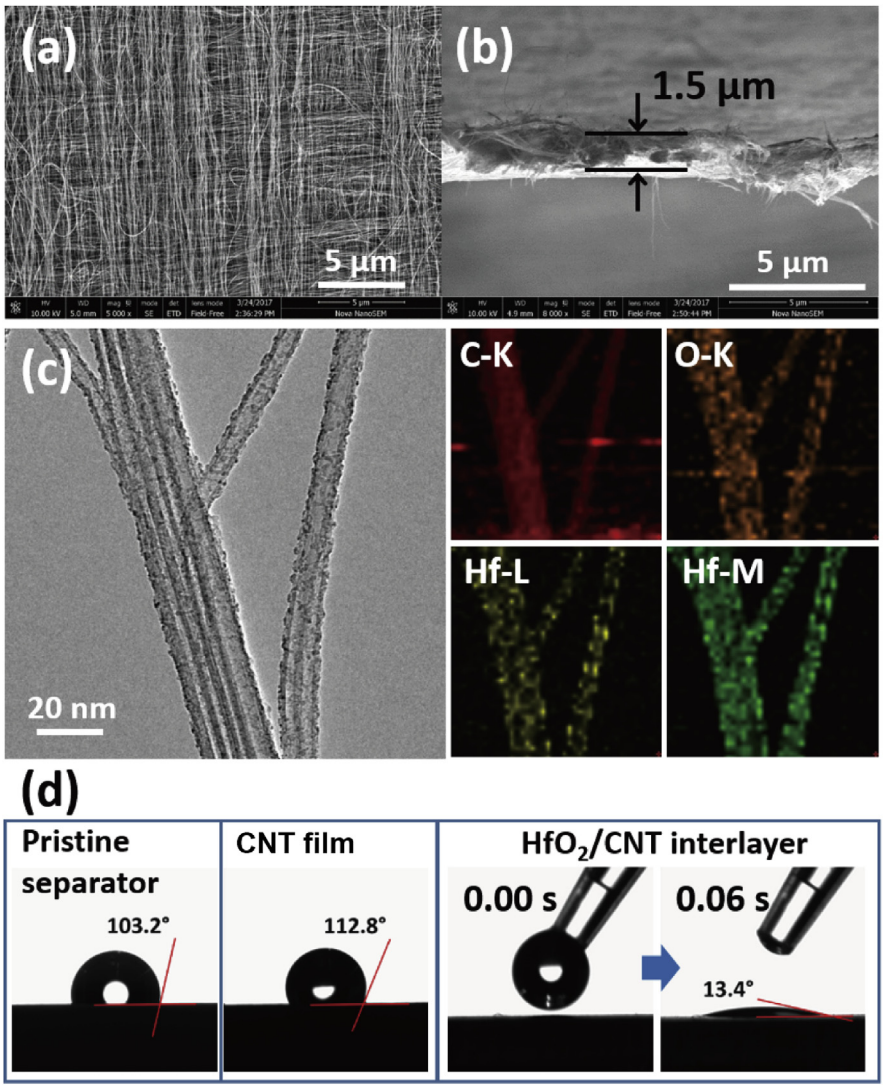

Fig. 2. SEM images of the (a) top surface and (b) cross-section of a HfO_2/CNT interlayer. (c) TEM image and EDX mapping of a HfO_2/CNT interlayer. (d) Wettability tests of a pristine separator, CNT film, and HfO_2/CNT interlayer. (A colour version of this figure can be viewed online.)

As shown in Fig. 2d, 1.5 μL of deionized water was dropped on a pristine separator, CNT film, and HfO_2/CNT interlayer, respectively. Due to the nonpolar properties of the pristine separator and CNT film, the contact angles were 103.2° and 112.8°, respectively. The inferior wettability of the separator/interlayer would be expected to hinder Li ion transport and interfacial electrochemical processes. In the case of the HfO_2/CNT interlayer, the oxygen defects and HfO_2 layer modification greatly improved the surface interaction between the interlayer and solvents, and the contact angle decreased to 13.4°. The excellent wettability of the HfO_2/CNT interlayer would significantly increase the quantity of active sites available for electrochemical reactions between the active materials and electrolyte. Moreover, the highly polar polysulfides could be effectively adsorbed by the HfO_2/CNT interlayer.

Fig. 3 shows the morphologies of CNTs coated using 14, 21, and 35 ALD cycles. After 14 ALD cycles, the CNTs were covered with a uniform HfO_2 layer having a thickness of less than 2 nm (Fig. 3a). As the deposition process increased to 21 cycles, the thickness of the HfO_2 layer increased to 3 nm (Fig. 3b). In the case of the HfO_2/CNT composite made with 35 ALD cycles, the CNTs were evenly coated with a 5 nm thick HfO_2 layer (Fig. 3c). The introduction of the HfO_2 layer potentially promoted the polysulfide trapping ability of the film, although the insulating nature of the HfO_2 could also result in slower electrochemical kinetics. Fig. 3d demonstrates the cycling performance of the electrodes made with a pristine separator, a CNT film, and HfO_2/CNT interlayers fabricated using 14, 21, or 35 ALD cycles. With the stepwise introduction of the CNT film and the HfO_2/CNT interlayer, the cycling stabilities of the electrodes were greatly improved. Due to the effective surface catalytic adsorption of the HfO_2/CNT interlayer, polysulfide diffusion was also reduced significantly. The electrode with the HfO_2/CNT interlayer made with 21 ALD cycles demonstrated the best performance, with a specific capacity as high as 1275 mA h g^{-1}. After 100 cycles at 0.2 C (1 C = 1672 mA g^{-1}), the discharge capacity remained at 995 mA h g^{-1}, showing good cycling stability. These results confirmed that the HfO_2 modification effectively alleviated the shuttle effect. In addition, the CNT network promoted the surface catalytic reaction of polysulfides due to the large surface area and excellent conductivity of the network. However, when the number of growth cycles applied during formation of the HfO_2 layer was increased to 35, the electrode demonstrated inferior performance with rapid capacity fading. An excess of HfO_2 hindered the charge

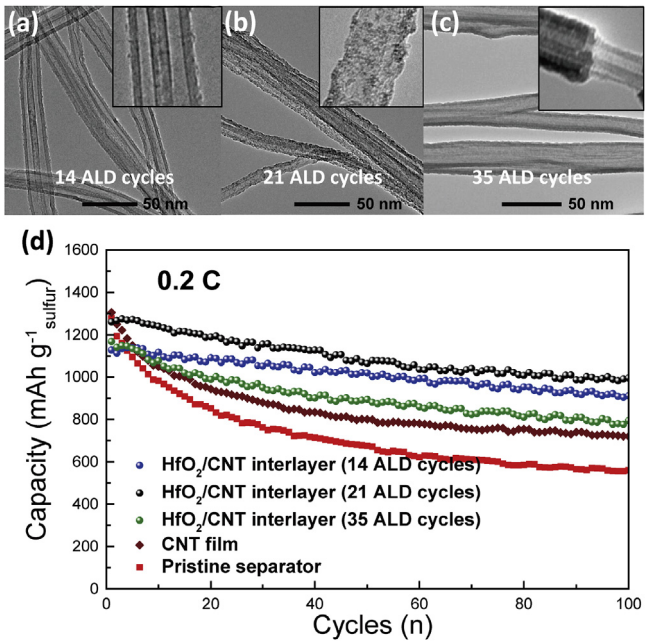

Fig. 3. TEM images of HfO_2/CNT composites with different HfO_2 coating thicknesses obtained following (a) 14, (b) 21, and (c) 35 ALD cycles. (d) Cycling performances of electrodes (S: 65 wt%) with the pristine separator, CNT film and HfO_2/CNT interlayers fabricated using various numbers of ALD cycles. (A colour version of this figure can be viewed online.)

transfer process, leading to the poor electrochemical performance. Therefore, in this study, the HfO_2 growth process was evidently optimized at 21 ALD cycles, which achieved a balance between the polysulfide trapping effect and the electrode conductivity.

The TGA results (Fig. S4) show that the sulfur contents of the electrodes were 65 and 75 wt%, with the sulfur areal densities ranging from 1.80 to 2.22 mg cm^{-2}. The cycling performances of the sulfur electrodes having a HfO_2/CNT interlayer and a pristine separator at 0.2 C are shown in Fig. 4a. The cell with the pristine separator exhibited an initial discharge capacity of 750 mA h $g^{-1}_{electrode}$ (S: 65 wt%) based on the overall electrode mass. However, after 100 cycles at 0.2 C, the capacity faded to only 378 mA h $g^{-1}_{electrode}$, showing a serious loss of the active material. At a sulfur content of 75 wt%, the slower reaction kinetics and greater degree of polysulfide diffusion led to an even lower initial discharge capacity of 105 mA h $g^{-1}_{electrode}$. Despite a slow increase in the following cycles, the capacity remained less than 400 mA h $g^{-1}_{electrode}$. The voltage profiles of the electrode having a pristine separator in Fig. S5a indicate poor redox kinetics with degraded discharge voltage plateaus. With the introduction of the HfO_2/CNT interlayer, the cycling performance of the electrode was greatly improved, especially at a high sulfur loading (Fig. 4a). Based on the mass of the entire electrode, the electrodes with 65 wt% and 75 wt% sulfur concentrations demonstrated initial discharge capacities of 723 and 836 mA h $g^{-1}_{electrode}$, respectively, while the capacities remained at 633 and 662 mA h $g^{-1}_{electrode}$ after 100 cycles at 0.2 C. These results confirm that polysulfide diffusion was effectively restrained by the HfO_2/CNT interlayer. The well-overlapped charge/discharge voltage profiles also demonstrate that the HfO_2/CNT interlayer resulted in stable reversibility of the redox reaction (Fig. S5b). Thus, the excellent conductivity provided by the cross-stacked CNT network and the adsorption of polysulfides by the HfO_2 allowed the electrode with the HfO_2/CNT interlayer to efficiently suppress the shuttle effect.

The rate capabilities of the sulfur electrodes with the HfO_2/CNT interlayer and the pristine separator were investigated at different charge/discharge current densities (Fig. 4b). The electrode with the HfO_2/CNT interlayer produced high discharge capacities of 1255, 1107, 1014, 970, 918, and 800 mA h g^{-1} at 0.2, 0.5, 1, 2, 3, and 5 C, respectively. More importantly, a discharge capacity of 1087 mA h g^{-1} could be recovered and stabilized when the current density returned to 0.5 C, showing an excellent reversible capacity retention of 98.2% over a series of high-rate tests. On the contrary, the electrode with the pristine separator presented much inferior rate performance. As the current density increased to 2 C, the discharge capacity faded to only 201 mA h g^{-1}. Afterwards, the cell was cycled at 0.5 C and showed a discharge capacity of 510 mA h g^{-1}, with a poor capacity retention of 57.8%.

Fig. 4c presents the charge/discharge voltage profiles of the sulfur electrode with the HfO_2/CNT interlayer at various current densities. The discharge process could be divided into two parts: the high voltage part (~2.35 V) associated with the conversion from cyclo-S_8 to polysulfides, and the low voltage part (~2.10 V) associated with the major discharge process from polysulfides to Li_2S_2/Li_2S. Because of the effective polysulfide trapping by the HfO_2/CNT interlayer, the electrode exhibited stable voltage plateaus as the current density increased, reflecting the improved redox kinetics. The discharge capacity retention of the high voltage part (Q_H) is typically used to evaluate the utilization of polysulfides [3,14]. As the current density increased, Q_H of the electrodes with the HfO_2/CNT interlayer maintained almost constant values in the vicinity of 392 mA h g^{-1}, indicating the strong polysulfide trapping capability of the HfO_2/CNT interlayer. In contrast, the high discharge voltage plateaus of the electrode with the pristine separator degraded severely as the current density increased to 2 C (Fig. 4d). A large amount of polysulfides evidently dissolved into the electrolyte and the further conversion to Li_2S_2/Li_2S can hardly proceed at high rates. The cyclic voltammetry (CV) profiles of the electrodes with the HfO_2/CNT interlayer and the pristine separator are shown in Fig. S6. The electrode with the HfO_2/CNT interlayer showed sharp and symmetric redox peaks. The reduction peaks at 2.32 V and 2.04 V corresponded to two discharge processes of the electrode ($S_8 \rightarrow Li_2S_4$ and $Li_2S_4 \rightarrow Li_2S_2/Li_2S$), and two oxidation peaks at 2.34 V and 2.40 V represented the aforementioned reverse conversions. Due to the effective polysulfide trapping of the HfO_2/CNT interlayer, the hysteresis of the redox peaks was only 0.296 V, showing relatively small polarization of the sulfur cathode. On the contrary, the electrode with the pristine separator showed degraded redox peaks, demonstrating a poor electrochemical kinetics and severe polarization.

The long-term cycling stability of the sulfur electrode with the HfO_2/CNT interlayer was investigated and the results are shown in Fig. 4e. A high discharge capacity of 721 mA h g^{-1} was obtained after 500 cycles at 1 C and the capacity fading was only −0.064% per cycle. In addition, the coulombic efficiency remained close to 98.4%, indicating a stable charge/discharge process. Conversely, the electrode with the pristine separator showed rapid capacity fading. Due to the continuous diffusion of polysulfides between the electrodes, as well as increasing corrosion of the Li anode, the electrode demonstrated a much lower discharge capacity of less than 600 mA h g^{-1} after 150 cycles and failed at the 280th cycle. The capacity fluctuation observed for the cells with the HfO_2/CNT interlayer or pristine separator was mainly caused by the temperature changes inside the laboratory [47].

The HfO_2/CNT interlayer also contributed to a notable improvement in the anti-self-discharge behavior of the electrodes. Generally, the dissolution of active sulfur during a prolonged rest period results in significant self-discharge as the polysulfides diffuse to the Li anode [3,5,48]. As can be seen from Fig. 5a, the electrode with the pristine separator exhibited a low capacity

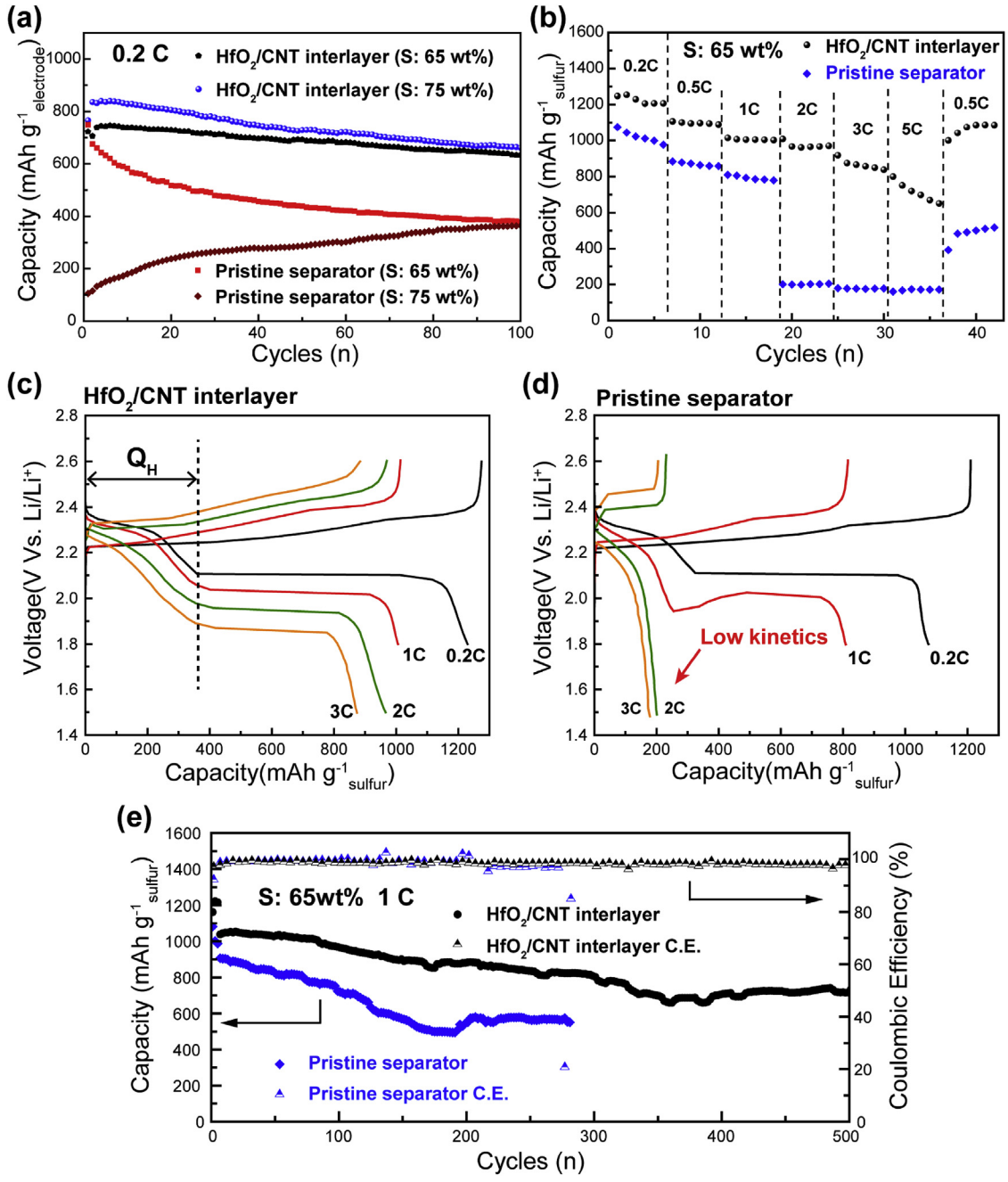

Fig. 4. (a) Cycling performances of electrodes with the HfO_2/CNT interlayer and the pristine separator at sulfur concentrations of 65 wt% and 75 wt% at 0.2 C. (b) Rate performances of electrodes with the HfO_2/CNT interlayer and the pristine separator at a sulfur concentration of 65 wt%. Voltage profiles of electrodes with (c) the HfO_2/CNT interlayer and (d) the pristine separator at different charge/discharge rates. (e) Long-term cycling performances of electrodes (1 C, S: 65 wt%) with the HfO_2/CNT interlayer and the pristine separator. (A colour version of this figure can be viewed online.)

retention of 64.5% after 20 days rest following initial cycling at 0.2 C for 20 cycles, and the discharge capacity remained at less than 600 mA h g^{-1} during additional cycling to 100 cycles. However, the electrode with the HfO_2/CNT interlayer exhibited superior anti-self-discharge capability. Under the same conditions, the capacity retention after 20 days rest was 90.8%, while the discharge capacity remained at nearly 1000 mA h g^{-1}. Fig. 5b presents the voltage profiles of the electrode with the HfO_2/CNT interlayer before and after 20 days rest. The smooth voltage plateaus overlapped appreciably, indicating the highly reversible redox kinetics of the electrode. The Q_H of the cell after 20 days rest was maintained at 89.9%, reflecting the efficient polysulfide trapping ability of the HfO_2/CNT interlayer. In contrast, pronounced self-discharge resulting from polysulfide dissolution was apparent in the case of the electrode with the pristine separator (Fig. 5c), along with severe capacity decay and voltage hysteresis. In addition, the Q_H dropped to only 63.1% after 20 days rest, indicating poor utilization of polysulfides.

In Li-S batteries, the shuttled polysulfides react with the Li anode, resulting in rapid capacity fading and the growth of a passivation layer [10,19,48]. The solid electrolyte interface (SEI) film on the Li anode can be destroyed by side-reactions with these

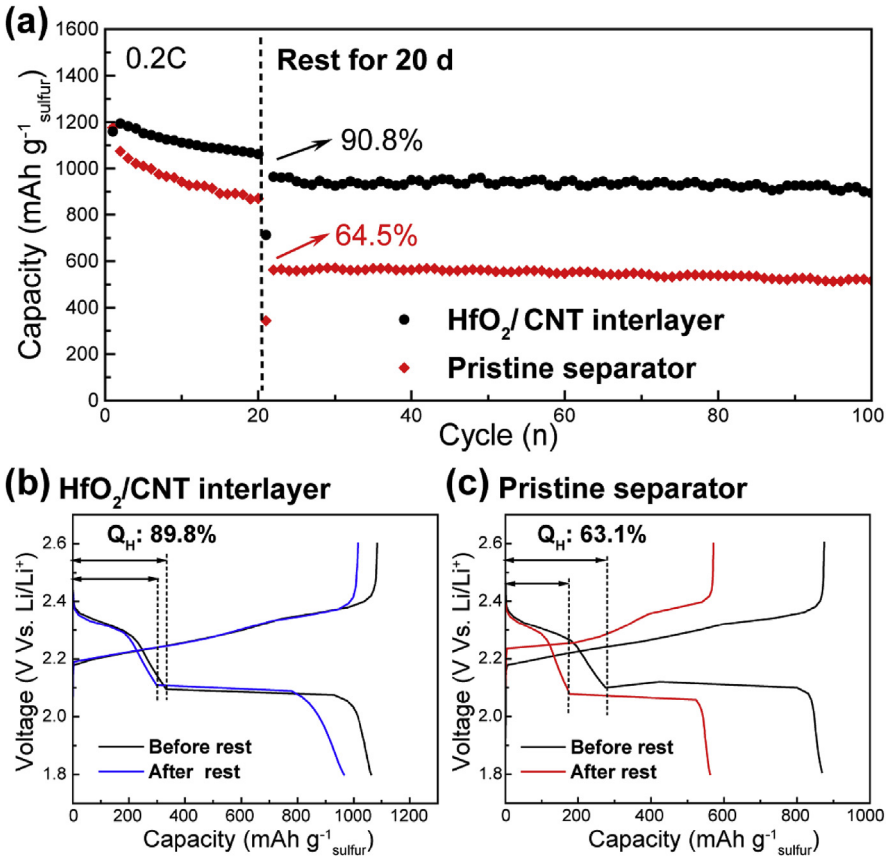

Fig. 5. (a) Cycling performances of electrodes with the HfO_2/CNT interlayer and the pristine separator with 20 days resting time after 20 cycles at 0.2 C. Charge/discharge voltage profiles of electrodes with (b) the HfO_2/CNT interlayer and (c) the pristine separator before/after 20 days rest. (A colour version of this figure can be viewed online.)

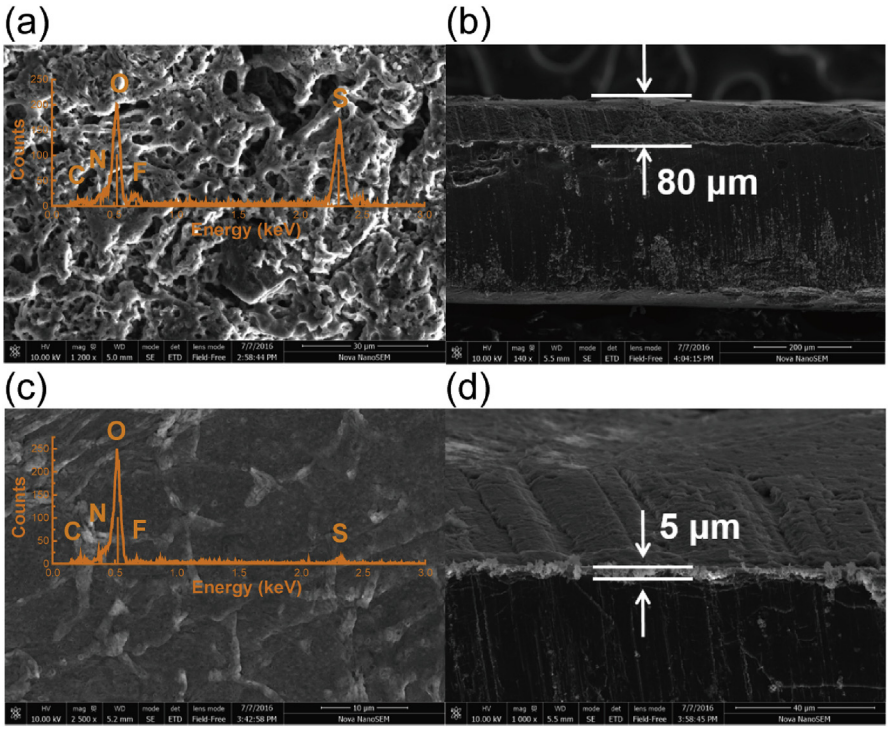

Fig. 6. Top surface and cross-sectional SEM images of the cycled Li anodes with (a, b) the pristine separator and (c, d) the HfO_2/CNT interlayer. The inset images show the corresponding EDX spectra. (A colour version of this figure can be viewed online.)

polysulfides, leading to severe surface corrosion and the formation of so-called “dead Li” or “dead S.” As shown in Fig. 6a, the SEM image of the top surface of the cycled Li anode with the pristine separator had a very rough morphology due to corrosion. The EDX spectrum (inset to Fig. 6a) indicated high S and O concentrations, and demonstrated that the surface passivation layer was primarily composed of lithium sulfides and electrolyte additives. The cross-sectional SEM image shows that the passivation layer was nearly 80 μm thick (Fig. 6b), which could lead to high internal resistance and poor redox kinetics. In contrast, the cycled Li anode of the cell with the HfO_2/CNT interlayer presented a much smoother surface morphology and the EDX spectrum indicated a relatively low sulfur content, confirming that the SEI film was well protected by the HfO_2/CNT interlayer (Fig. 6c). From the cross-sectional morphology in Fig. 6d, it is apparent that the passivation layer on the Li anode was only 5 μm thick. Owing to the significant polysulfide trapping by the HfO_2 nanocoating, the Li anode surface corrosion was greatly alleviated, thus promoting the utilization of active materials and long-term cyclic stability (Fig. 4e).

To more thoroughly investigate the surface catalytic adsorption process resulting from the HfO_2 modification, XPS spectra were acquired from the HfO_2/CNT interlayer before and after cycling. Fig. S7 presents the typical XPS survey spectrum of the HfO_2/CNT interlayer, exhibiting the characteristics peaks of Hf 4f (17 eV), Hf 4d (213 eV), Hf 4p (381 eV), C 1s (285 eV), and O 1s (532 eV). The C 1s narrow peak (calibrated by C-C bond at 284.8 eV) is shown in Fig. S8, in which the hydroxyl groups (-C-O) at 286.6 eV and carboxyl (ester) groups (-C=O) at 288.6 eV were revealed. These functional groups were mainly generated from the RIE treatment of CNT, and provided continuous adsorption sites for HfO_2 growth. Fig. 7a shows the high resolution XPS spectrum of the HfO_2/CNT interlayer before cycling. The Hf 4f core level could be deconvoluted to give a single Hf $4f_{7/2}$ - Hf $4f_{5/2}$ doublet with a fixed area ratio of 4:3 and a doublet separation of 1.64 eV. The binding energy of Hf $4f_{7/2}$ in the HfO_2 layer was 16.78 eV, and this value could have been affected by many factors, including the charge transfer effect, environmental charge density and hybridization [43,49]. Fig. 7b presents the XPS spectrum of the HfO_2/CNT interlayer after cycling, showing a 0.42 eV decrease in binding energy. This shift is ascribed to the charge transfer process between the polysulfides and the HfO_2 layer. The S 2p spectrum and the fitted components of the HfO_2/CNT interlayer after cycling are given in Fig. 7c. The S 2p core level was deconvoluted to give S $2p_{3/2}$ - S $2p_{1/2}$ doublets with a fixed area ratio of 2:1 and a doublet separation of 1.16 eV. The two components at 161.7 and 163.4 eV correspond to the S $2p_{3/2}$ signals from terminal sulfur, S_T^{-1}, and bridging sulfur, S_B^0, respectively, both of which originate from long-chain polysulfides [36–38]. The doublet at 166.8 eV corresponds to the thiosulfate species generated by the surface adsorption reaction between the polysulfides and the HfO_2 layer. The doublet at 168.6 eV is assigned to the polythionate species that result from the further reaction between the polysulfides and thiosulfate species. Fig. 7c demonstrates that the long-chain polysulfides were converted to thiosulfate and polythionate species, confirming the interfacial catalytic reaction at the surface of the HfO_2/CNT interlayer. This interfacial adsorption process was accompanied by a decrease in the Hf 4f binding energy (Fig. 7b), demonstrating that the polysulfides were efficiently trapped via thiosulfate-polythionate conversion upon introducing the HfO_2 nanolayer. Moreover, the excellent conductivity of the CNT network greatly accelerated the interfacial reaction, thus improving the electrochemical kinetics of the electrode.

To visually examine the adsorption capacity of the HfO_2/CNT interlayer, the cycled cells were detached, and the S-CNT electrodes were soaked in DOL/DME solution with a volume ratio of 1:1 (Fig. S9). The liquid with the electrode and the HfO_2/CNT interlayer was much more transparent than that with the electrode and the pristine separator, indicating a strong polysulfide-trapping capability of the HfO_2/CNT interlayer. Furthermore, TEM morphology and EDS mapping of the HfO_2/CNT interlayer after cycling are shown in Fig. S10. The evenly distributed signals of Hf, O, and S demonstrated favorable stability of the HfO_2/CNT interlayer. The synergy between the HfO_2 modification and CNT network is illustrated in Fig. 7d. The HfO_2 nanolayer provided an effective polysulfide trapping mediator. In addition, the CNT network served as a physical barrier to prevent polysulfides diffusion as well as an efficient electron transport pathway to enhance the interfacial adsorption of the polysulfide utilization.

An Al_2O_3/CNT interlayer was also fabricated by ALD as a

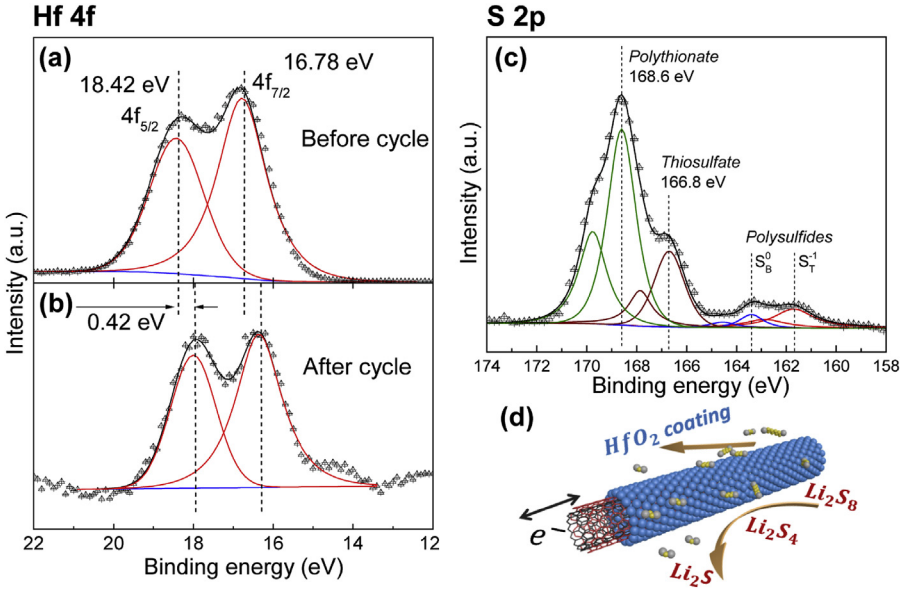

Fig. 7. High-resolution Hf 4f XPS spectra of the HfO_2/CNT interlayer (a) before and (b) after the cycling test. (c) High-resolution S 2p XPS spectrum of the HfO_2/CNT interlayer after the cycling test. (d) Schematic illustration of the surface adsorption process between the HfO_2/CNT interlayer and polysulfides. (A colour version of this figure can be viewed online.)

comparison, and Fig. S11 presents the cycling performances of the electrodes with the HfO_2/CNT and Al_2O_3/CNT interlayers. Compared with Al_2O_3, HfO_2 exhibited more efficient catalytic adsorption of polysulfides, and the electrode with the HfO_2/CNT interlayer showed a more stable discharge capacity during cycling tests. Comprehensive criteria for the selection of oxides include effective binding, a high surface area, and good surface diffusion properties, since monolayer chemisorption is dominant during the polysulfides conversion process [50]. In the case of the HfO_2/CNT interlayer, the deposition of the HfO_2 nanolayer can be precisely controlled using the ALD technique, thus greatly offsetting its low conductivity and optimizing the specific surface area. Compared with other metal oxides, such as MnO_2, HfO_2 avoids side-reactions in the voltage window applied, thus more efficiently trapping polysulfides [19,36]. Moreover, the excellent wettability and conductivity of the CNT network greatly increases the effective surface area and accelerates the catalytic conversion of long-chain polysulfides. Therefore, the electrochemical performance of the sulfur electrode with the HfO_2/CNT interlayer was significantly improved.

4. Conclusion

In summary, a multi-functional HfO_2/CNT interlayer is proposed as an efficient polysulfide barrier for advanced Li-S batteries. With an ultrathin film structure (1.5 μm) and a low areal density (0.087 mg cm^{-2}), the interlayer delivers excellent improvements in various electrochemical properties, including long-term cycling stability (721 mA h g^{-1} after 500 cycles at 1 C), high rate charge/discharge performance (800 mA h g^{-1} at 5 C), anti-self-discharge capability, and protection of the Li anode. The binder-free sulfur electrode permits high sulfur loadings, up to 75 wt%, and is extremely flexible while not requiring a current collector. As a result of the HfO_2/CNT interlayer, a superior capacity value of 836 mA h $g^{-1}_{electrode}$ (0.2 C) was obtained based on the entire electrode, which is greater than values reported for conventional sulfur cathodes. The excellent electrochemical performance of sulfur electrodes with the HfO_2/CNT interlayer is ascribed to the enhanced polysulfide utilization originating from the highly conductive CNT network as well as catalytic adsorption by the HfO_2 in the HfO_2/CNT interlayer, as confirmed by XPS analysis. These results suggest a new approach to the design of effective polysulfide barriers and high-performance Li-S batteries.

Acknowledgements

This work was supported by National Natural Science Foundation of China (51472141) and by the National Key Research and Development Program of China (2017YFA0205800). JL acknowledges support by NSF ECCS-1610806.

Appendix A. Supplementary data

Supplementary data related to this article can be found at https://doi.org/10.1016/j.carbon.2018.07.063.

References

[1] M. Armand, J.-M. Tarascon, Building better batteries, Nature 451 (2008) 652–657.
[2] N. Nitta, F. Wu, J.T. Lee, G. Yushin, Li-ion battery materials: present and future, Mater. Today 18 (2015) 252–264.
[3] A. Manthiram, Y. Fu, S.H. Chung, C. Zu, Y.S. Su, Rechargeable lithium-sulfur batteries, Chem. Rev. 114 (2014) 11751–11787.
[4] Y. Yang, G. Zheng, Y. Cui, Nanostructured sulfur cathodes, Chem. Soc. Rev. 42 (2013) 3018–3032.
[5] M. Hagen, D. Hanselmann, K. Ahlbrecht, R. Maça, D. Gerber, J. Tübke, Lithium-sulfur cells: the gap between the state-of-the-art and the requirements for high energy battery cells, Adv. Energy Mater. 5 (2015) 1401986.
[6] M.A. Pope, I.A. Aksay, Structural design of cathodes for Li-S batteries, Adv. Energy Mater. 5 (2015) 1–22.
[7] J.T. Lee, H. Kim, M. Oschatz, D.C. Lee, F. Wu, H.T. Lin, B. Zdyrko, W. Il Cho, S. Kaskel, G. Yushin, Micro- and mesoporous carbide-derived carbon-selenium cathodes for high-performance lithium selenium batteries, Adv. Energy Mater. 5 (2015) 1–7.
[8] B. Zhang, X. Qin, G.R. Li, X.P. Gao, Enhancement of long stability of sulfur cathode by encapsulating sulfur into micropores of carbon spheres, Energy Environ. Sci. 3 (2010) 1531.
[9] G. He, X. Ji, L. Nazar, High "C" rate Li-S cathodes: sulfur imbibed bimodal porous carbons, Energy Environ. Sci. 4 (2011) 2878.
[10] G. Zhou, Y. Zhao, A. Manthiram, Dual-confined flexible sulfur cathodes encapsulated in nitrogen-doped double-shelled hollow carbon spheres and wrapped with graphene for Li-S batteries, Adv. Energy Mater. 5 (2015) 1–10.
[11] N. Jayaprakash, J. Shen, S.S. Moganty, A. Corona, L.A. Archer, Porous hollow Carbon@Sulfur composites for high-power lithium–sulfur batteries, Angew. Chem. Int. Ed. 50 (2011) 5904–5908.
[12] J. Guo, Y. Xu, C. Wang, Sulfur-impregnated disordered carbon nanotubes cathode for lithium-sulfur batteries, Nano Lett. 11 (2011) 4288–4294.
[13] T. Xu, J. Song, M.L. Gordin, H. Sohn, Z. Yu, S. Chen, D. Wang, Mesoporous carbon – carbon nanotube – sulfur composite microspheres for high-areal-capacity lithium – sulfur battery cathodes, ACS Appl. Mater. Interfaces 5 (2013) 11355–11362.
[14] W. Kong, L. Sun, Y. Wu, K. Jiang, Q. Li, J. Wang, S. Fan, Binder-free polymer encapsulated sulfur-carbon nanotube composite cathodes for high performance lithium batteries, Carbon 96 (2016) 1053–1059.
[15] H. Wang, Y. Yang, Y. Liang, J.T. Robinson, Y. Li, A. Jackson, Y. Cui, H. Dai, Graphene-Wrapped sulfur particles as a rechargeable lithium – sulfur battery cathode material with high capacity and cycling stability, Nano Lett. 11 (2011) 2644–2647.
[16] R. Chen, T. Zhao, J. Lu, F. Wu, L. Li, J. Chen, G. Tan, Y. Ye, K. Amine, Graphene-based three-dimensional hierarchical sandwich-type architecture for high-performance Li/S batteries, Nano Lett. 13 (2013) 4642–4649.
[17] L. Fei, X. Li, W. Bi, Z. Zhuo, W. Wei, L. Sun, W. Lu, X. Wu, K. Xie, C. Wu, H.L.W. Chan, Y. Wang, Graphene/sulfur hybrid nanosheets from a space-confined "sauna" reaction for high-performance lithium-sulfur batteries, Adv. Mater. 27 (2015) 5936–5942.
[18] L. Sun, M. Li, Y. Jiang, W. Kong, K. Jiang, J. Wang, S. Fan, Sulfur nanocrystals confined in carbon nanotube network as a binder-free electrode for high performance lithium sulfur batteries, Nano Lett. 14 (2014) 4044–4049.
[19] W. Kong, L. Yan, Y. Luo, D. Wang, K. Jiang, Q. Li, S. Fan, J. Wang, Ultrathin MnO 2/graphene oxide/carbon nanotube interlayer as efficient polysulfide-trapping shield for high-performance Li-S batteries, Adv. Funct. Mater. 27 (2017) 1606663.
[20] L. Sun, D. Wang, Y. Luo, K. Wang, W. Kong, Y. Wu, L. Zhang, K. Jiang, Q. Li, Y. Zhang, J. Wang, S. Fan, Sulfur embedded in a mesoporous carbon nanotube network as a binder-free electrode for high-performance lithium-sulfur batteries, ACS Nano 10 (2016) 1300.
[21] K. Jiang, Q. Li, S. Fan, Nanotechnology: spinning continuous carbon nanotube yarns, Nature 419 (2002) 801.
[22] K. Liu, Y. Sun, L. Chen, C. Feng, X. Feng, K. Jiang, Y. Zhao, S. Fan, Controlled growth of super-aligned carbon nanotube arrays for spinning continuous unidirectional sheets with tunable physical properties, Nano Lett. 8 (2008) 700–705.
[23] S. Luo, K. Wang, J. Wang, K. Jiang, Q. Li, S. Fan, Binder-free LiCoO 2/carbon nanotube cathodes for high-performance lithium ion batteries, Adv. Mater. 24 (2012) 2294–2298.
[24] K. Wang, S. Luo, Y. Wu, X. He, F. Zhao, J. Wang, K. Jiang, S. Fan, Super-aligned carbon nanotube films as current collectors for lightweight and flexible lithium ion batteries, Adv. Funct. Mater. 23 (2013) 846–853.
[25] J.Q. Huang, Q. Zhang, F. Wei, Multi-functional separator/interlayer system for high-stable lithium-sulfur batteries: progress and prospects, Energy Storage Mater. 1 (2015) 127–145.
[26] J.-Q. Huang, Q. Zhang, H.-J. Peng, X.-Y. Liu, W.-Z. Qian, F. Wei, Ionic shield for polysulfides towards highly-stable lithium–sulfur batteries, Energy Environ. Sci. 7 (2014) 347.
[27] C. Li, A.L. Ward, S.E. Doris, T.A. Pascal, D. Prendergast, B.A. Helms, Polysulfide-blocking microporous polymer membrane tailored for hybrid Li-Sulfur flow batteries, Nano Lett. 15 (2015) 5724–5729.
[28] J. Balach, T. Jaumann, M. Klose, S. Oswald, J. Eckert, L. Giebeler, Functional mesoporous carbon-coated separator for long-life, high-energy lithium-sulfur batteries, Adv. Funct. Mater. 25 (2015) 5285–5291.
[29] H. Bin Yao, K. Yan, W. Li, G. Zheng, D. Kong, Z.W. Seh, V.K. Narasimhan, Z. Liang, Y. Cui, Improved lithium-sulfur batteries with a conductive coating on the separator to prevent the accumulation of inactive S-related species at the cathode-separator interface, Energy Environ. Sci. 7 (2014) 1–10.
[30] Y.-S.S. Su, A. Manthiram, A new approach to improve cycle performance of rechargeable lithium-sulfur batteries by inserting a free-standing MWCNT interlayer, Chem. Commun. 48 (2012) 8817–8819.
[31] S. Chung, A. Manthiram, High-performance Li – S batteries with an ultra-lightweight MWCNT- coated separator, J. Phys. Chem. Lett. 5 (2014) 1978–1983.
[32] J.Q. Huang, T.Z. Zhuang, Q. Zhang, H.J. Peng, C.M. Chen, F. Wei, Permselective graphene oxide membrane for highly stable and anti-self-discharge lithium-

sulfur batteries, ACS Nano 9 (2015) 3002–3011.
[33] Z. Xiao, Z. Yang, L. Wang, H. Nie, M. Zhong, Q. Lai, X. Xu, L. Zhang, S. Huang, A lightweight TiO2/graphene interlayer, applied as a highly effective polysulfide absorbent for fast, long-life lithium– sulfur batteries - SI, Adv. Mater. 27 (2015) 2891–2898.
[34] Z. Zhang, Y. Lai, Z. Zhang, K. Zhang, J. Li, Al2O3-coated porous separator for enhanced electrochemical performance of lithium sulfur batteries, Electrochim. Acta 129 (2014) 55–61.
[35] Z.A. Ghazi, X. He, A.M. Khattak, N.A. Khan, B. Liang, A. Iqbal, J. Wang, H. Sin, L. Li, Z. Tang, MoS_2/Celgard separator as efficient polysulfide barrier for long-life lithium-sulfur batteries, Adv. Mater. (2017) 1606817.
[36] X. Liang, C.Y. Kwok, F. Lodi-Marzano, Q. Pang, M. Cuisinier, H. Huang, C.J. Hart, D. Houtarde, K. Kaup, H. Sommer, T. Brezesinski, J. Janek, L.F. Nazar, Tuning transition metal oxide-sulfur interactions for long life lithium sulfur batteries: the "goldilocks" principle, Adv. Energy Mater. 6 (2016) 1501636.
[37] X. Liu, J.-Q. Huang, Q. Zhang, L. Mai, Nanostructured metal oxides and sulfides for lithium-sulfur batteries, Adv. Mater. 29 (2017) 1601759.
[38] X. Liang, C. Hart, Q. Pang, A. Garsuch, T. Weiss, L.F. Nazar, A highly efficient polysulfide mediator for lithium–sulfur batteries, Nat. Commun. 6 (2015) 5682.
[39] Y. Zhou, C. Zhou, Q. Li, C. Yan, B. Han, K. Xia, Q. Gao, J. Wu, Enabling prominent high-rate and cycle performances in one lithium-sulfur battery: designing permselective gateways for Li+ transportation in holey-CNT/S cathodes, Adv. Mater. 27 (2015) 3774–3781.
[40] Z. Yuan, H.J. Peng, T.Z. Hou, J.Q. Huang, C.M. Chen, D.W. Wang, X.B. Cheng, F. Wei, Q. Zhang, Powering lithium-sulfur battery performance by propelling polysulfide redox at sulfiphilic hosts, Nano Lett. 16 (2016) 519–527.
[41] S.S. Zhang, D.T. Tran, Pyrite FeS_2 as an efficient adsorbent of lithium polysulphide for improved lithium–sulphur batteries, J. Mater. Chem. A 4 (2016) 4371–4374.
[42] B. Ahmed, D.H. Anjum, M.N. Hedhili, H.N. Alshareef, Mechanistic insight into the stability of HfO2-coated MoS2 nanosheet anodes for sodium ion batteries, Small 11 (2015) 4341–4350.
[43] N. Yesibolati, M. Shahid, W. Chen, M.N. Hedhili, M.C. Reuter, F.M. Ross, H.N. Alshareef, SnO2 anode surface passivation by atomic layer deposited HfO2 improves li-ion battery performance, Small 10 (2014) 2849–2858.
[44] P. Arora, Z. Zhang, Battery separators, Chem. Rev. 104 (2004) 4419–4462.
[45] J.Q. Huang, Q. Zhang, S.M. Zhang, X.F. Liu, W. Zhu, W.Z. Qian, F. Wei, Aligned sulfur-coated carbon nanotubes with a polyethylene glycol barrier at one end for use as a high efficiency sulfur cathode, Carbon 58 (2013) 99–106.
[46] H. Wei, J. Ma, B. Li, Y. Zuo, D. Xia, Enhanced cycle performance of lithium -sulfur batteries using a separator modified with a PVDF-C layer, ACS Appl. Mater. Interfaces 6 (2014) 20276–20281.
[47] R. Ye, J. Bell, D. Patino, K. Ahmed, M. Ozkan, C.S. Ozkan, Advanced sulfur-silicon full cell architecture for lithium ion batteries, Sci. Rep. 7 (2017) 1–10.
[48] R. Cao, W. Xu, D. Lv, J. Xiao, J.G. Zhang, Anodes for rechargeable lithium-sulfur batteries, Adv. Energy Mater. 5 (2015) 1–23.
[49] M.H. Cho, Y.S. Roh, C.N. Whang, K. Jeong, S.W. Nahm, D.H. Ko, J.H. Lee, N.I. Lee, K. Fujihara, Thermal stability and structural characteristics of HfO2 films on Si (100) grown by atomic-layer deposition, Appl. Phys. Lett. 81 (2002) 472–474.
[50] X. Tao, J. Wang, C. Liu, H. Wang, H. Yao, G. Zheng, Z.W. Seh, Q. Cai, W. Li, G. Zhou, C. Zu, Y. Cui, Balancing surface adsorption and diffusion of lithium-polysulfides on nonconductive oxides for lithium–sulfur battery design, Nat. Commun. 7 (2016) 11203.